

A GUIDE TO THE MAIN RING DØ OVERPASS

Frank Turkot

March 20, 1985

I. Introduction

The DØ overpass is a modification of the beam orbit in Main Ring in order to better accommodate a Tevatron collider detector at DØ. The orbit is moved up ~51 inches over most of the long straight section at DØ, thus making the Main Ring the world's first non-planar proton synchrotron. A similar overpass, but with four times the displacement, is planned for the CDF detector at the BØ straight section.

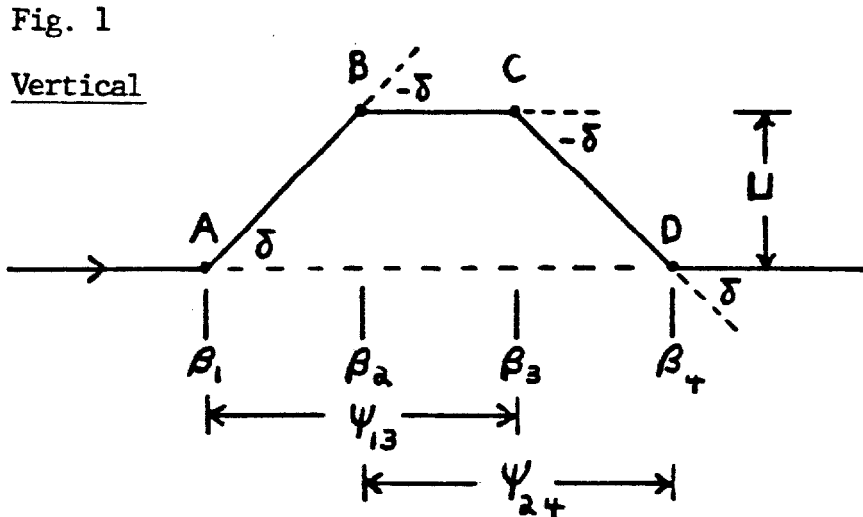
The nominal separation between the beam orbit in the Main Ring and the orbit in the Tevatron is 25.5 inches. Early in the design study of a detector that would utilize the Tevatron as a $\bar{p}p$ collider, it was apparent that a larger separation at the detector was highly desirable. In 1981, Tom Collins (Ref. 1) proposed a specific lattice geometry in the Main Ring for achieving larger separation, called "the screw beam". His proposal has served as the basis for the design of both the BØ and DØ overpasses.

The main purpose of this report is to describe in some detail the implementation of the DØ overpass. Topics to be covered include: (a) geometry of the overpass orbit, (b) the new hardware in the tunnel, (c) the power supply system, (d) the control facility, (e) accelerator beam

dynamics ramifications, and (f) commissioning experience. A secondary purpose is to provide a fairly complete "bibliography" to the sources of information on the overpass.

II. The Collins Overpass Scheme

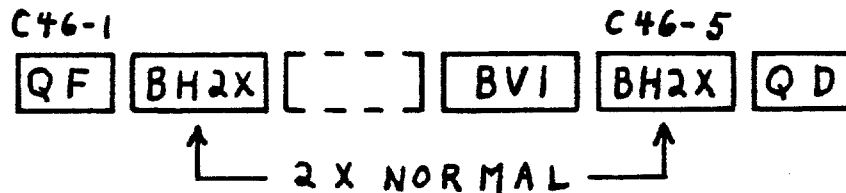
The vertical path of the closed orbit in the Collin's proposal is shown schematically in Figure 1.



The vertical displacement of the orbit by amount U is accomplished by four identical bends by angle δ . The introduction of the vertical bends into the previously planar Main Ring lattice results in a non-zero vertical momentum dispersion, η_y ($\Delta y = \eta_y \Delta p/p$, Δy is the deviation from the central orbit due to a momentum deviation $\Delta p/p$). If the values of vertical beta function, β_y , at the four bend locations are equal and if the phase advance of the vertical betatron motion satisfies, $\psi_{13} = \psi_{24} = 360^\circ$, then one obtains the desirable feature, $\eta_y = 0$ in the rest of the ring outside of the overpass region.

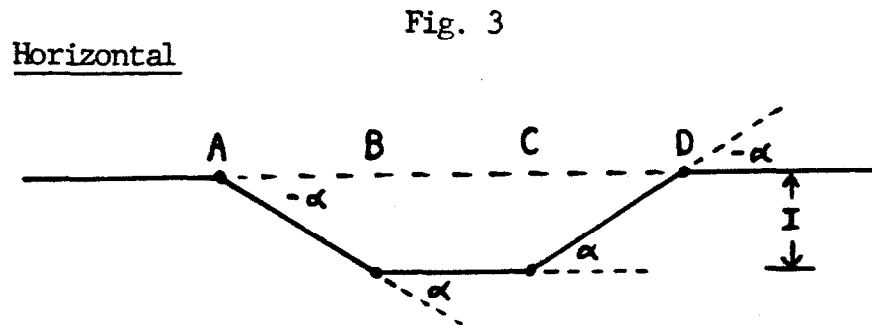
The vertical bend δ is substantial, for $D\theta \delta \sim 16$ mrad (a standard Main Ring dipole bends through $2\pi/774 = 8.12$ mrad). Space for the vertical bends in the lattice is created by limiting the Main Ring operation to less than 200 GeV. Figure 2 shows the lattice half-cell containing the first vertical bend for the $D\theta$ overpass.

Fig. 2



The two horizontal dipoles at locations C46-3 and C46-4 have been removed; the two horizontal dipoles at C46-2 and C46-5 are run at twice normal field, thus keeping the total bend and the horizontal bend center of the half-cell the same. There is then space to insert a vertical dipole at C46-4; the C46-3 slot is left empty.

The addition of the vertical bump as in Figure 1 will increase the total path length in the overpass region and hence the total path length around the accelerator. To maintain the central orbit and phase stability, any change in path length must be an integral number of RF wavelengths ($\lambda_{RF} \sim 222$ inches). At $D\theta$ (and $B\theta$) the change in path length is small compared to λ_{RF} and is made zero by simultaneously making a horizontal, radially-inward bump in the overpass region as in Figure 3.



The most efficient way to effect this bump is to roll the dipoles used to create the vertical bump.

Ignoring the vertical dipoles, the region A to D of Figure 1. has not only the same path length as the unperturbed Main Ring, but also has the same quads and dipoles with the same spacing between magnets along the new central orbit. It seems plausible then, that except for $\eta_y \neq 0$, the lattice functions of the Main Ring with overpass will be very close to the unperturbed ring. The curve of the central orbit in regions A to B and C to D of Figure 1 approximates a helix (the "screw beam"); in the ascending region A to B it is a left-handed screw, and in the descending region C to D, it is a right-handed screw.

Figure 4 shows the geometry of one of the dipoles in region A B; the central orbit enters the dipole at the origin perpendicular to \vec{B} , with pitch angle δ with respect to the horizontal plane xy , and at an angle $\phi/2$ w.r.t. the long axis of the dipole (ϕ is the bending angle of

FIG. 4

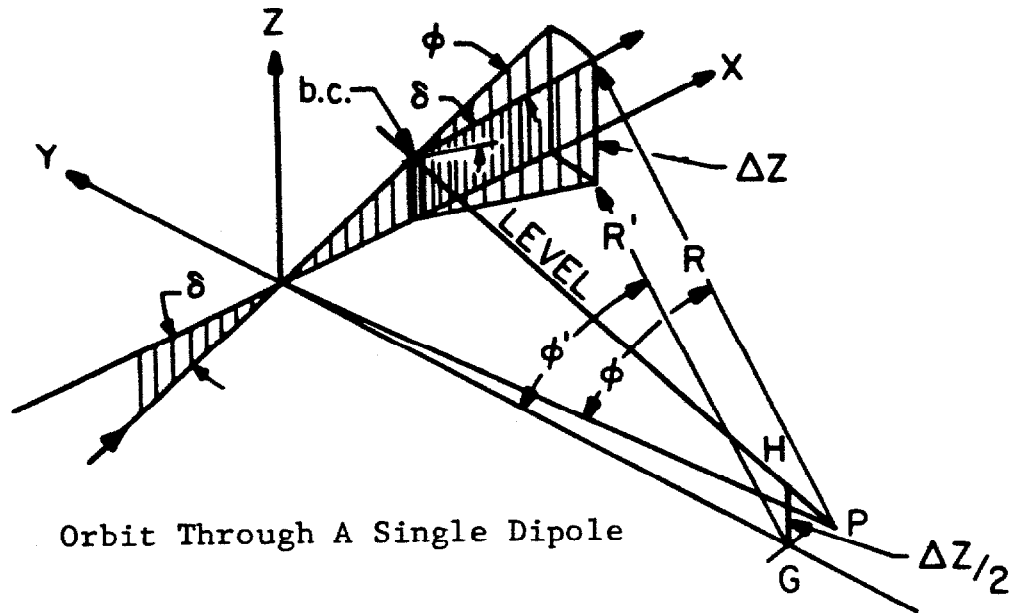
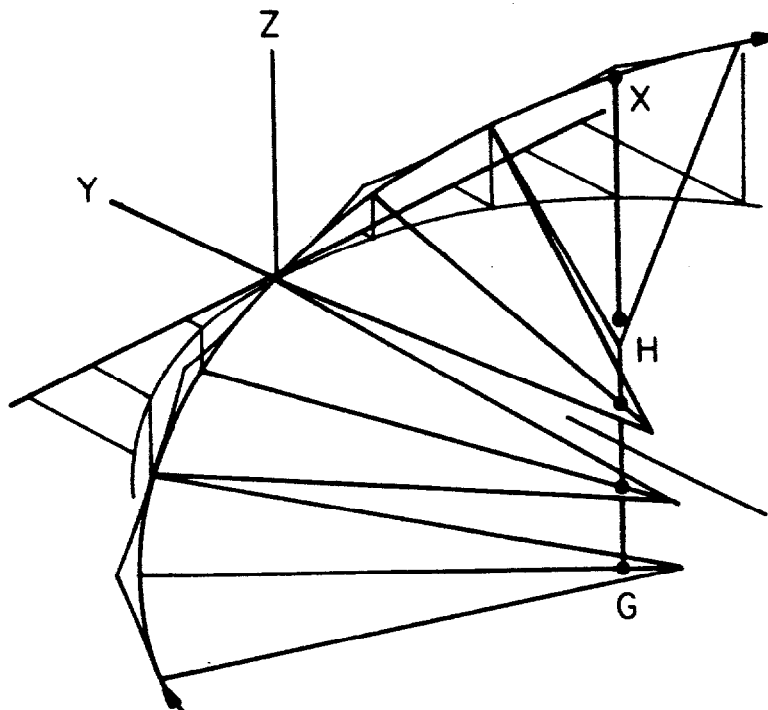


FIG. 5

Left-handed Dipole Sequence



the dipole). The dipole has zero roll and a pitch δ' , slightly larger than δ . The beam is bent through an angle ϕ in the bend plane of the dipole, bend radius R , with center of curvature P at a height $\Delta z/2$ above the xy plane. The beam leaves the magnet with pitch angle δ at elevation Δz ; the projection of the orbit into the xy plane is a piece of a circle of radius R' (the radius of the screw), center at G and with angle ϕ' . The line HG is the axis of the screw and is parallel to the z axis. For small ϕ , these quantities are related as follows:

$$R' = R \cos^2 \delta \quad (1)$$

$$\phi' = \phi / \cos \delta \quad (2)$$

$$\delta' = \delta / \cos \phi/2 \quad (3)$$

$$\Delta z = R\phi \sin \delta \quad (4)$$

The next dipole is placed with pitch δ' , zero roll, but with \vec{B} rotated around HG by an angle ϕ' . The quads are placed with their axes along the beam (hence pitch δ) and with zero roll. Figure 5 shows a sequence of dipoles making an orbit that approximates a helix; the centers of curvature of the dipoles fall on a second helix having the same pitch and axis as the beam helix but with radius $R - R'$.

This geometry has the nice feature - from the practical point of view of magnet placement - that all quads and dipoles have the same pitch and zero roll; the most obvious alternative geometry, the "great circle" (Ref.1), has different pitch and roll for every magnet in the overpass region. An overpass with screw geometry will introduce

coupling between vertical and horizontal betatron motion, but it should be small compared to other sources (see Sect. X. below).

III. The DØ Overpass Geometry

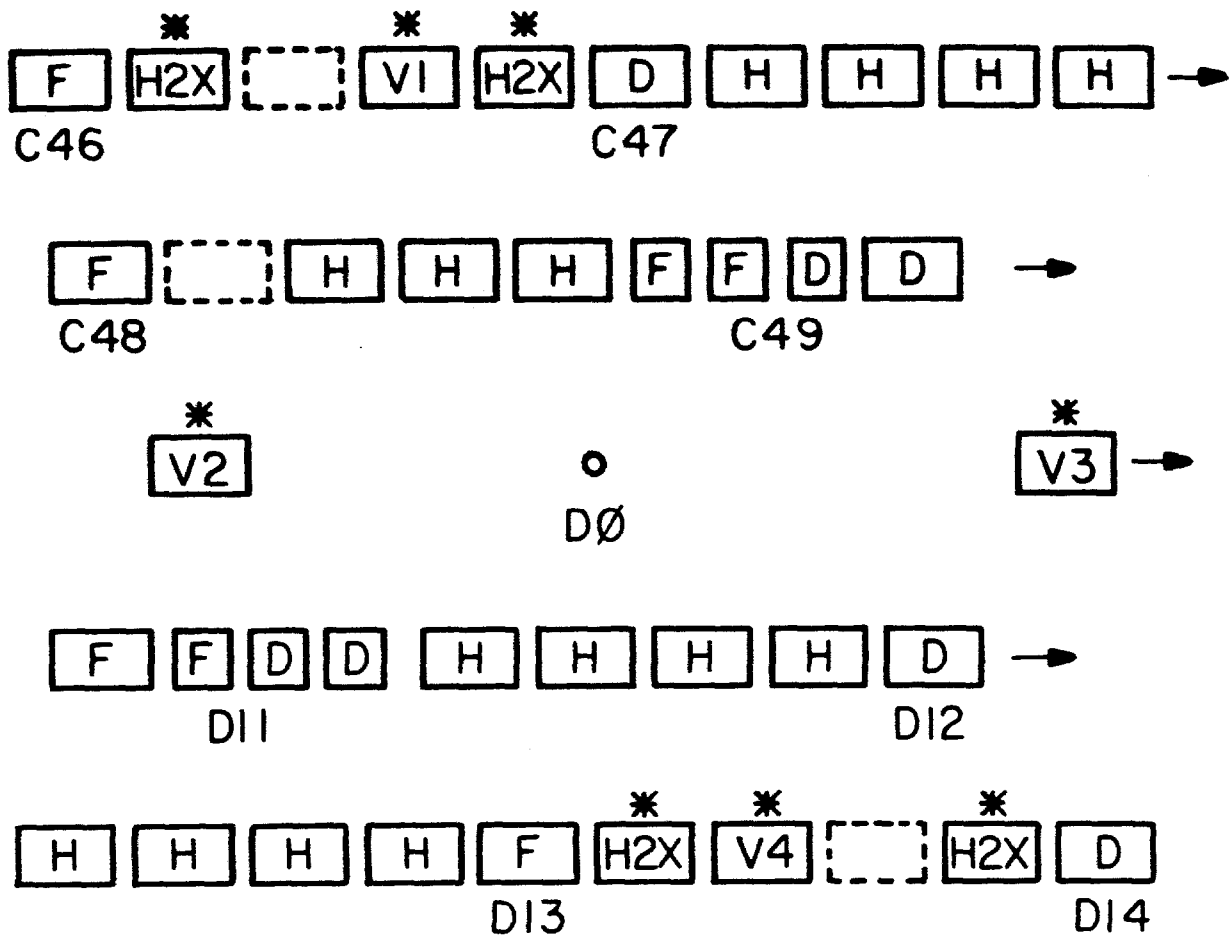
The basic geometry of the overpass now installed at DØ was proposed by S. Ohnuma in August of 1983 (Ref. 2); it bears the label "Wildman's dream." It utilizes the screw geometry as proposed by T. Collins but ignores the condition $\Delta\psi = 360^\circ$; one of the boundary conditions imposed was that the existing tunnel (outside of the DØ straight section) not be disturbed, a condition that limits the vertical displacement of the beam at DØ to .50 inches.

Once the sequence of the magnets and the overpass height are chosen, the detailed magnet positions are determined by a computer program which transports the beam element by element through the overpass. It is important that the new orbit "close" to the old orbit at the end of the overpass with high precision in both vertical and horizontal dimensions; the parameters available are the roll angles of the four vertical bends, perfect closure requires two small additional vertical bends (Ref. 2). Closure is obtained by iterative passes through the geometry program called "DSCREWF", written by S. Ohnuma.

The magnet sequence for the DØ overpass is given in Figure 6; it extends from the first bend downstream of C46 quad to the bend just upstream of D14 quad, a distance of 786 feet (3.8% of the accelerator circumference). The insertion of the first up-bend at the C46-4 location was described above (Section II, Figure 2); the two down-bends

FIG. 6

Magnet Sequence In The DØ Overpass



* Magnets In Series On Overpass Bus

are inside the D0 long straight, the second up-bend is inserted at D13-D14 (a mirror image about D0 of the C46-C47 half cell).

The overpass geometry currently in place at D0, goes under the name "WD51D2" (Ref. 3), the vertical and horizontal projections of the overpass orbit are shown in Figure 7; the distances shown are actually path lengths along the orbit from bend centers. The four vertical dipoles BV1 - BV4, are identical and designed to have a bend angle twice that of a standard Main Ring horizontal dipole, $2 \times 2\pi/774 = 16.24$ mrad. The design roll angles of the magnets are (\vec{B} w.r.t. the horizontal);

BV1	BV2	BV3	BV4
0.24150	-0.24150	-0.24291	0.24170 rad.

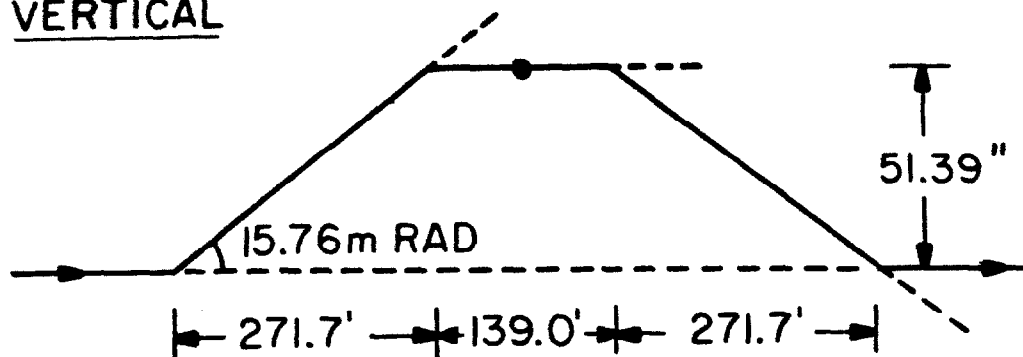
If the dipoles were not rolled, i.e. no horizontal bump, then the path length through the overpass would be 0.87 in. longer than that of the original orbit. At D0, between BV2 and BV3, the overpass orbit is horizontal but not quite parallel to the unperturbed Main Ring orbit due to the helical path between BV1 and BV2 (see Eq.(2)).

As indicated the pitch angle of the beam, and hence of the quads also, is 15.76 mrad. The dipole pitch is given by eq.(3)

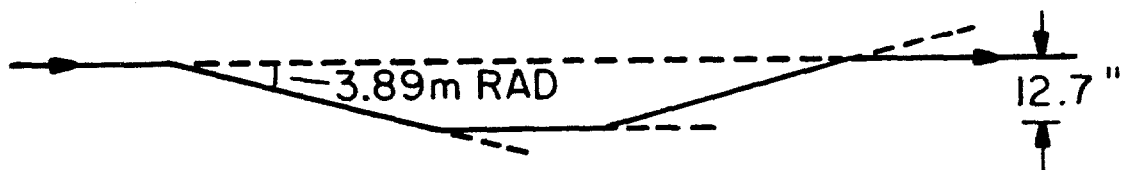
$$\delta' = \delta / \cos \phi/2$$

hence δ' differs from δ by 1 part in 3×10^4 , which is much smaller than achievable setting errors of the dipoles.

FIG. 7

DØ OVERPASS - WD51 (D2)VERTICAL

ψ	0°	90°	124°	206°
β	63.3	110.8	51.1	48.7m
η_y	1.18	-0.31	-0.00	1.08m

HORIZONTAL

ψ	0°	82°	116°	206°
β	44.6	51.9	115.1	58.7m
η_x	1.57	1.87	3.03	1.55m

IV. Overpass Tunnel Hardware

The D0 overpass region involves repositioning 35 main magnets, (Fig.6) 23 bend magnets and 12 quads, plus the fast horizontal kicker at C48-2 which is used to transfer protons from Main Ring to Tevatron. Of these 35 magnets, 29 have a common non-zero pitch, and the four BV's have a roll of $\sim 14^\circ$. For a 239 inch-long dipole the pitch amounts to a 3.766 inch change in elevation from end to end and for a 7 foot quad a change of 1.324 inches. The most numerous new hardware elements are the new magnet stands, which vary in size to allow for different magnet elevations and radial repositioning, as much as 13 inches closer to the tunnel center line. A special effort was made in the magnet alignment for the overpass region (Ref. 3). Pitch angles were set with a precision of ± 0.08 mrad; roll angles on the vertical bends were set to ± 0.25 mrad and for the other magnets to ± 0.5 mrad.

The four vertical bend magnets are a new design, they have a beam aperture of 2.8 inches in the field direction and 4.7 inches transverse. Their physical length is 236.9", the calculated (Ref. 4) effective length at 14 KG is 240 inches. For the overpass parameters, the operating design field at 150 GeV/c is 13.32 KG at a current (parallel connection of coils) of 3375a, nominally twice the field of a standard Main Ring dipole at 150 GeV/c. The magnet also has a 20-turn trim coil (24 turn main coil) which enables a 50 a current to make a $\pm 1.2\%$ field change at 150 GeV/c.

Finally, there is a new pair of 1.5 inch water-cooled bend buses running from C46-1 (fold end) to D15-1 and then up to the service

building (see Sect. V). The four BV magnets and the four BH2X are in the new bus system. The remaining 27 magnets of the overpass remain on their original Main Ring bus.

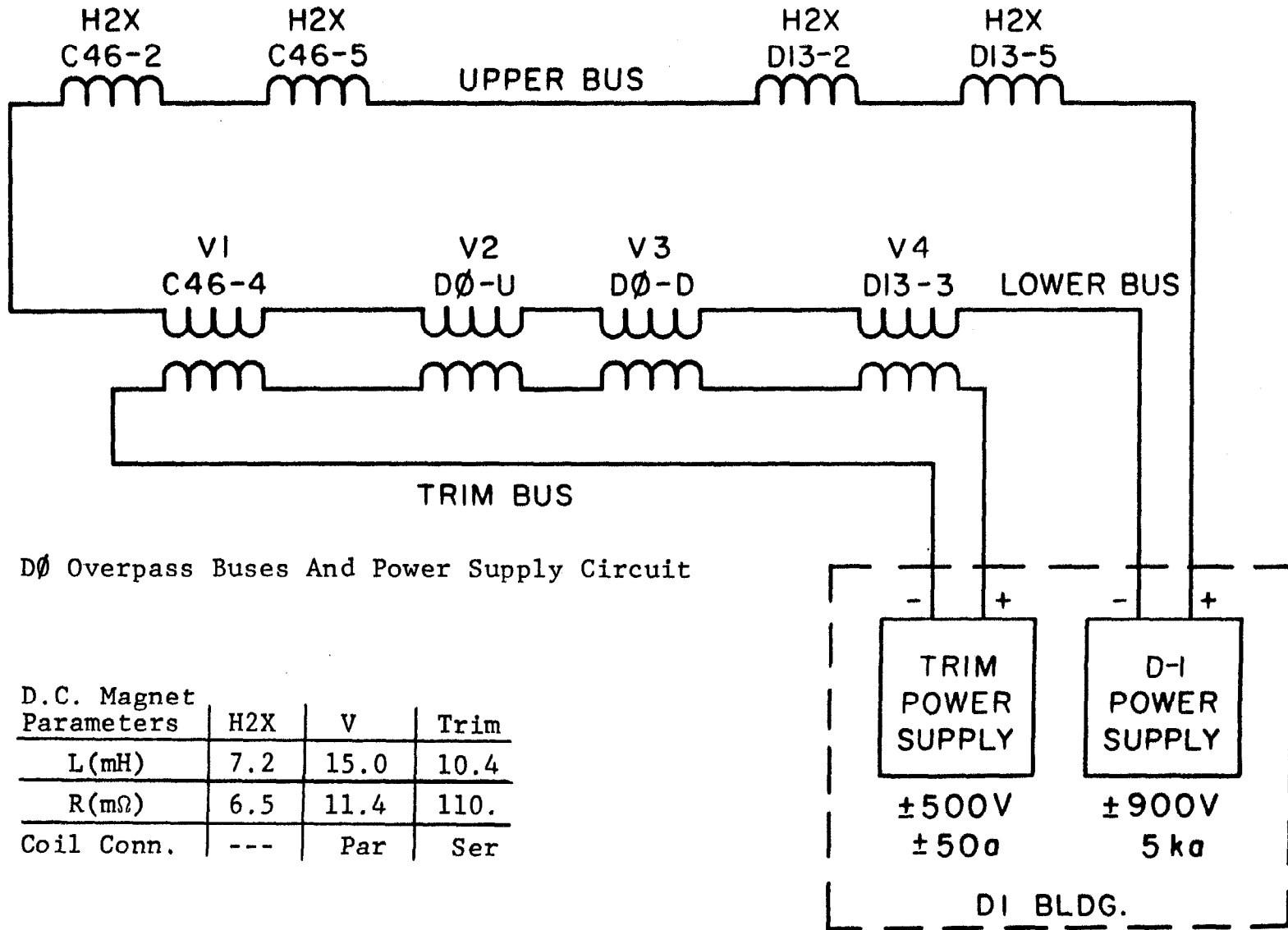
V. Overpass Power Supply System

The power supplies, bus, and magnet configuration are exhibited on Fig. 8 (Ref. 5). The supply labeled D1 is a pair of Main Ring power supplies (formerly UD1 and LD1); they are in series on the bus, but only one of the two is used in normal operation. To first approximation, the main bus operates at twice the current of the Main Ring bus, hence it cycles between 193a at 8.9 GeV/c to 3400a at 150 GeV/c. All 8 overpass dipoles have twice the field, B , and twice dB/dt compared to a standard Main Ring bend; for example at an acceleration of 120 GeV/c per second they will have dB/dt of 10.7 kG/s and dI/dt of 2.70 ka/s. The overpass main bus has a total inductance and resistance of 90 mH and 88 m Ω , so at 120 GeV/c per second an inductive voltage of 248 V and at 150 GeV/c a resistive voltage of 299 V.

The trim windings on the vertical dipoles are put in series on a second bus (2/0 cable) and driven by a ± 500 V, ± 50 a power supply (a Tevatron Higher Order Correction Element Power Supply). The magnets present a transformer coupling between the two circuits, and therefore, modify the AC behavior of each.

The control and regulation scheme for the system is shown in Figure 9 (Ref. 5). The first order voltage program for the D1 main power supply is derived from a transducer on the Main Ring upper bend bus in the D1 building. Small changes, D \emptyset ADJ, to the current program are made

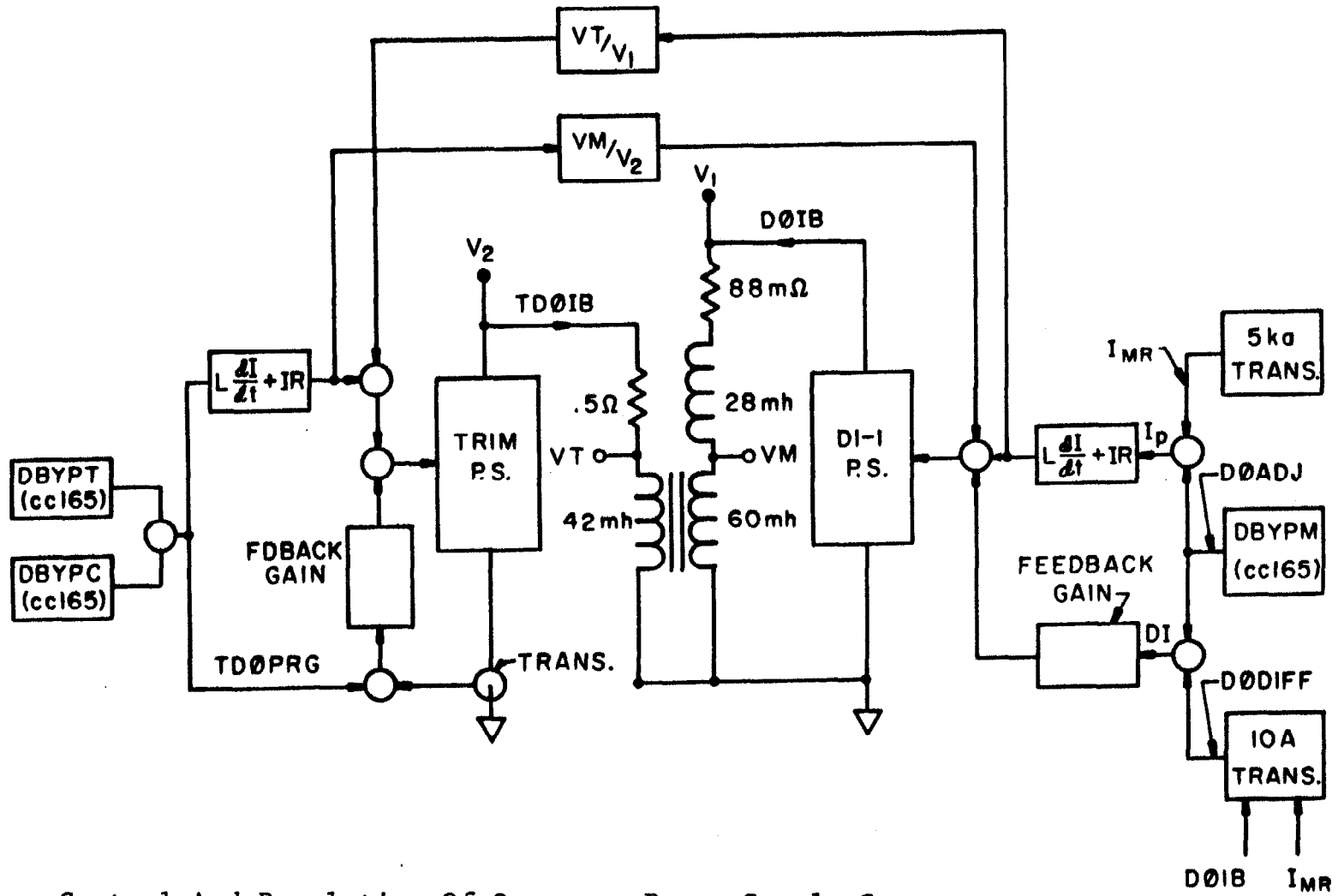
FIG. 8



DØ Overpass Buses And Power Supply Circuit

D.C. Magnet Parameters	H2X	V	Trim
L(mH)	7.2	15.0	10.4
R(mΩ)	6.5	11.4	110.
Coil Conn.	---	Par	Ser

FIG. 9



Control And Regulation Of Overpass Power Supply System

via a function generation card (a CC165) controlled by the Accelerator Control System. An error signal for current regulation is derived from D0ADJ and D0DIFF ($\equiv D0IB - 2 I_{MR}$); the latter signal produced by a triple-transducer system (Ref. 6) (D0IB is measured by a second transducer on the overpass bus in D1). Finally, there is AC feedback from the trim power supply to take into account the coupling.

For the trim power supply the current program, TD0PRG, is derived from a pair of CC165 cards; DBYPT supplies the main program and DBYPC a compensation that depends on current in the Tevatron bus. For regulation, the error signal TD0PRG-TD0IB is derived using a 50 a transducer on the trim bus. In a similar fashion there is feedback of the voltage program for the main supply to handle the coupling.

Specifications on the D1 main supply are:

- a) regulation of average current - $\pm 0.013\%$
- b) peak to peak current ripple - 0.35 a

The trim supply has stability and ripple $\leq 0.01\%$ of full scale current.

VI. Power Supply Control and Monitoring

The means for remote monitoring and control of the overpass power supplies is provided by the Accelerator Control System using three "application" programs (Ref. 7) currently residing at index page locations M33-35.

1. M34 - Supply Status and Control

The console monitor display for M34 is shown in Fig. 10(a); the "Gate Turn Off" is a switch in series with the trim power supply to protect it from large voltage transients which might occur due to unusual behavior of the main supply (see Fig. 9).

Fig. 10(a)

THU 07-MAR-85 10:44

M34 MAIN RING OVERPASS SUPPLY STATUS AND CONTROL

#LX# X-A/D X=TIME Y=MID01B ,MID01B ,MID01DIFF,MID01PRG
 15HZ Volts I= 0 I= 0 ; 0 ; 0
 F NR --- F= 8 F= 10 ; 10 ; 10 ; 10

MAIN SUPPLY RAMP CONTROL

#RAMP / #HALT
 #RESET
 Ramp/Halt Status.... HALT

RAMP INHIBITS.....

Fast Trip Loop..... TRIP
 Choke Temp..... OK
 Filter Temp..... OK
 Gate Turn Off Trip.. OK
 Trim PS Off..... OFF
 Ground Fault..... OK
 Overpass Overcurrent OK
 VCB Off..... OPEN
 Tunnel Klaxon..... OK

REGULATION STATUS.....

Reg. Out Of Limit... BAD

MAIN SUPPLY VCB CONTROL

 D1-1 D1-2
 Lockout # .
 Off .
 On .
 Fault .
 Over-I .

VCB INHIBITS.....

Permit Loop..... GONE
 Power Supply Doors.. CLSD
 Trim PS Door..... CLSD
 Battery Box..... BAD

TRIM SUPPLY CONTROL

#ON / #OFF
 #RESET

TRIPS.....

Permit..... GONE
 Doors..... CLSD
 Load Overcurrent... OK
 Circulating Cur. O/I OK
 PS Overvolts..... OK
 Ground Fault..... OK
 DC Contactor..... CLSD
 SCR Temperature..... OK
 DC Current Transactr OK
 Phase Rotation..... OK
 Gate Turn Off O/I... OK
 Gate Turn Off Temp.. OK
 GTD Resistor Temp... OK
 Transistor Regulator FLY
 AC Contactor..... OPEN
 Remote/Local..... RMT

Fig 10(b)

THU 07-MAR-85 10:47

M35 CC165 CONTROL
 #LX# X-A/D X=TIME Y=MIDODIFF,MIDOADJ ,MID01B ,MIDOPRG
 15HZ Volts I= 0 I=-6 , -6 , -20 , -20
 #MR .--. F= 8 F= 2 , 2 , 0 , 0

#SAVEPG
 #PS CONTROL / clock events / table control

VOUT = SF = E = G(T)

Power supply (MIDBYPM)

#Read ramp (3)
 #Load to ramp ()

Active ramps #1.(3) #2.(3) - #SET

#DAT #Enabled/ Disabled
 ramp #Enabled/ disabled

Ramp 1 scale factor = (.68)
 Ramp 1 slope = (0)

Ramp 2 scale factor = (.68)
 Ramp 2 slope = (0)

Card type is bipolar

#Display 165 devices

For triggers, see clock events subpage

	START	LEVEL	()
		4.082	()
2.	(1000)	(4.082	()
3.	(50)	(4.597	()
4.	(50)	(3.796	()
5.	(100)	(1.796	()
6.	(100)	(1	()
7.	(100)	(-.199	()
8.	(100)	(-.5	()
9.	(240)	(-.957	()
10.	(90)	(-.898	()
11.	(170)	(-.777	()
12.	(150)	(-.667	()
13.	(140)	(-.566	()
14.	(190)	(-.449	()
15.	(446)	(-.257	()
16.	(2200)	(-.257	()
17.	(400)	(4.082	()
18.	(0)	(0	()
19.	(0)	(0	()
Total time =		5.526 sec			

2. M35 - CC165 Control

This program (Fig. 10(b) gives monitor display) allows one to set the parameters of the three CC165 Camac modules which generate the current-versus-time programs in the overpass main bus and the vertical bend trim bus; the module names are DBYPM, DBYPT, and DBYPC. The first order program for the main supply is hard-wired to be $2 \times (I \text{ in MR bend bus})$; DBYPM allows one to deviate by $\pm 350a$ from this program. DBYPT is the main program for the trim bus and has a $\pm 50a$ range.

3. M33 - DØ Overpass Devices

This program is an adaptation of a "parameter page to display various signals from the power supply system, such as:

$$DØDIFF = I_{opass} - 2 I_{MR} \text{ (bend bus)}$$

$$DØADJ = \text{output of DBYPM}$$

$$DØIB = I_{opass}$$

$$TDØPRG = \text{output of DBYPT and DBYPC} \quad (5)$$

$$TDØIB = I_{opass} \text{ (trim bus)}$$

If the power supply system is working properly then one should see

$$DØDIFF = DØADJ$$

$$TDØIB = TDØPRG$$

VII. Effect of Overpass on Lattice Functions and Closed Orbits

1. Lattice Functions

Lattice functions for the Main Ring with the DØ overpass have been calculated by S. Ohnuma (Ref. 8) for $v_x = v_y = 19.40$. The horizontal and vertical β functions are indistinguishable (differ by less than

0.7%) from those of the standard SYNCH run for no overpass. The horizontal momentum dispersion is plotted in Fig. 11(a) (η_x vs beam position detector locations); the horizontal bump at D0 has broken the six-fold symmetry. The original η_x , which ranged between 1.21 m (near "22" locations) and 5.85 m (near "28" locations), is now modulated by a "free oscillation" of amplitude ± 0.43 m and hence dips to a low of 1.01 m near C23 and a peak of 6.25 m at C28.

As mentioned above the most dramatic change is the appearance of vertical momentum dispersion, which is plotted in Fig. 11(b). Outside of the overpass region it has the form

$$\eta_y(s) \propto \sqrt{\beta_y(s)} \cos(\psi_y(s) + \Delta) \quad (6)$$

where $\psi_y(s)$ is the vertical betatron phase. It's maximum value of 1.86 m occurs at the upstream end of the E0 long straight section.

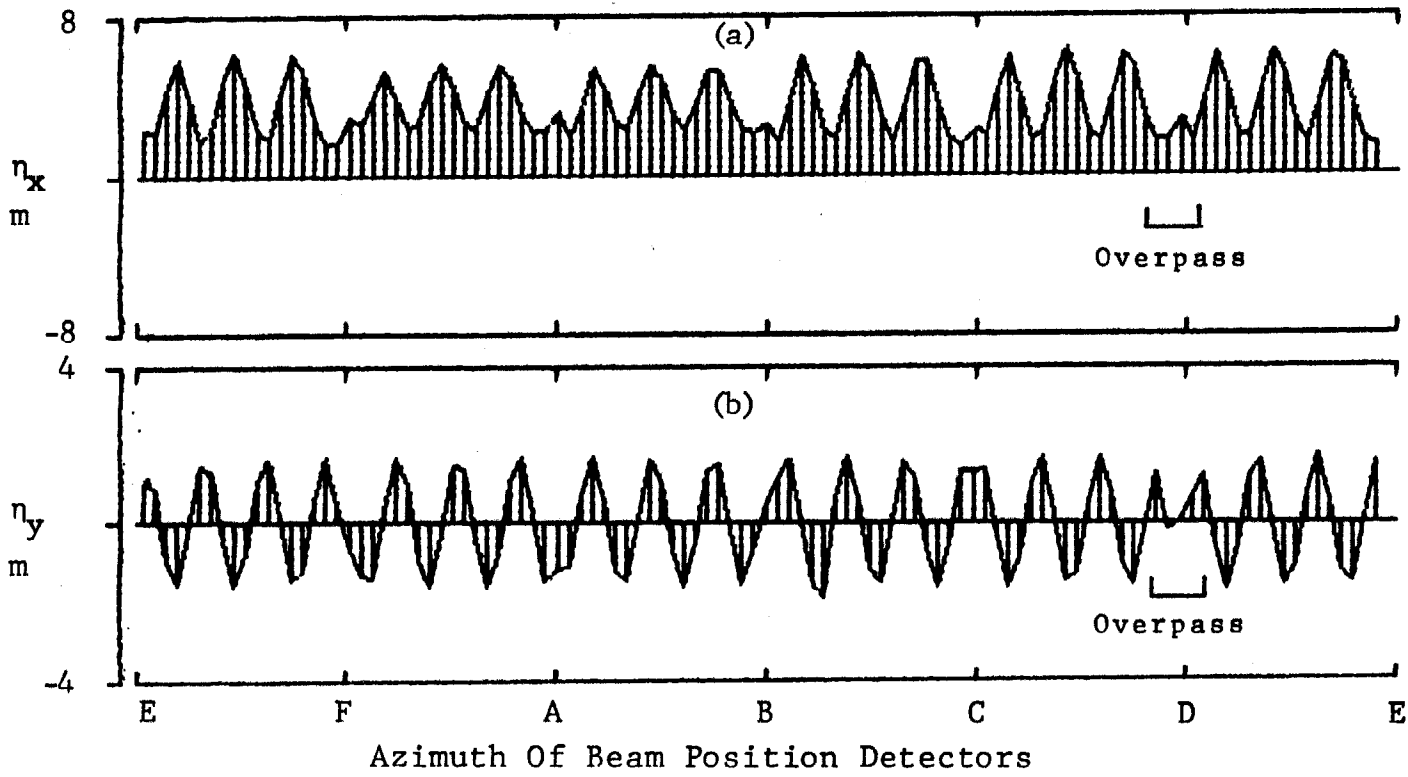
2. Closed Orbit Distortions

The overpass obviously creates a new closed orbit in the overpass region, however, if all of the magnets are properly located and have their design bend strengths, then the new closed orbit should be undistorted there and elsewhere around the ring.

If the currents in the either the main overpass bus (D0IB) or the trim bus (TD0IB) are in error then closed orbit distortions will result; at some beam position detector (at location "i") one will see

Fig. 11

Main Ring Momentum Dispersion Functions



$$x_i = D_{Hi} \delta_D + T_{Hi} \delta_{TH} \quad (7)$$

$$y_i = D_{Vi} \delta_D + T_{Vi} \delta_{TV}$$

where D_H is the horizontal distortion function due to the 8 dipoles (4 BH2X and 4 BV) on the main overpass bus and δ_D the fractional error in the bend angle of the BH2X magnets (assumes all 4 magnets are identical), i.e.

$$\delta_D = \frac{\theta - \theta_{\text{DESIGN}}}{\theta_{\text{DESIGN}}} = \frac{D\theta_{IB} - D\theta_{IB_0}}{D\theta_{IB_0}} \quad (8)$$

where $D\theta_{IB_0}$ is the current in the main bus that gives the design bend angle. Using the definition of Eq. (5)

$$D\theta_{DIFF_0} = D\theta_{IB_0} - 2 I_{MR}$$

it is straight forward to show that

$$D\theta_{DIFF_0} = - 2 I_{MR} \Delta(2 I_{MR}) \quad (9)$$

where $\Delta(I)$ is given by the field integrals for a standard MR bend magnet,

$$\Delta (2I) = \frac{1/2 \int B_y (2I) dl - \int B_y (I) dl}{\int B_y (I) dl} \quad (10)$$

Similarly T_H is the horizontal distortion function due to the 4 rolled BV's and

$$\delta_{TH} = \frac{\theta - \theta_{DESIGN}}{\theta_{DESIGN}} = \frac{TD\theta IB - TD\theta IB_{OH}}{1.2 D\theta IB_0} \quad (11)$$

The factor 1.2 arises from the fact that the trim winding has 20 turns, whereas the main coil has 24 (parallel connection). Similar to Eq. (9), one can derive a "zero distortion" value for $TD\theta IB_{OH}$ as

$$TD\theta IB_{OH} = - 1.2 (2 I_{MR}) (\zeta(2 I_{MR}) - 4\epsilon) \quad (12)$$

where $\zeta(I)$ now contains the field integral difference between a "standard" BV magnet (parallel coil connection) and a MR bend

$$\zeta(I) = \frac{\int_{BV} B_y (I) dl - \int_{MR} B_y (I) dl}{\int_{MR} B_y (I) dl} \quad (13)$$

The quantity ϵ is the systematic error (in radians, assuming all four magnets have the same error) in the roll angle,

$$\theta_{\text{ROLL}} = \theta_{\text{ROLL DESIGN}} + \epsilon \quad (14)$$

Similar comments apply to the vertical distortions; since the same four magnets (the BV's) are involved in both D_V and T_V , the functions are identical. In addition, the same magnets determine the vertical momentum dispersion η_y ; since $\Delta\theta/\theta > 0$ corresponds to a $\Delta p/p < 0$ we have the relation

$$D_{Vi} = T_{Vi} = - \eta_{yi} \quad (15)$$

Hence Eq. (7) becomes

$$y_i = - \eta_y (\delta_D + \delta_{TV}) \quad (16)$$

Taking $D\theta_{IB_0}$, we can show that the "zero distortion" value for the trim setting is

$$TD\theta_{IB_{0V}} = - 1.2 (2 I_{MR}) (\zeta(2 I_{MR}) + \epsilon/4) , \quad (17)$$

comparing with Eq. (12), one sees that the optimum trim settings for horizontal and vertical will differ in the presence of a systematic roll error of the vertical bends.

A distortion function due to a set of bend magnets on a common bus can be calculated from the lattice functions using the following formula (Ref. 9); at some location "i" (having β_i, ψ_i)

$$D_i = \frac{\sqrt{\beta_i}}{2 \sin \pi \nu} \sum_j \theta_j \sqrt{\beta_j} \cos (\psi_i - \psi_j - \pi \nu) \quad (18)$$

where β_j and ψ_j are at the location of the bend center of each magnet and θ_j is its design bend angle.

The functions D_{Hi} and T_{Hi} (Ref. 10) are plotted versus beam detector location in Fig. 12; it is interesting to note that outside of the overpass region (excluding HC48, HC49, HD11, and HD13) the two functions have nearly identical phase (differ by 3°) and D_H oscillates between ± 1.16 m, about 2.6 times the amplitude of T_H .

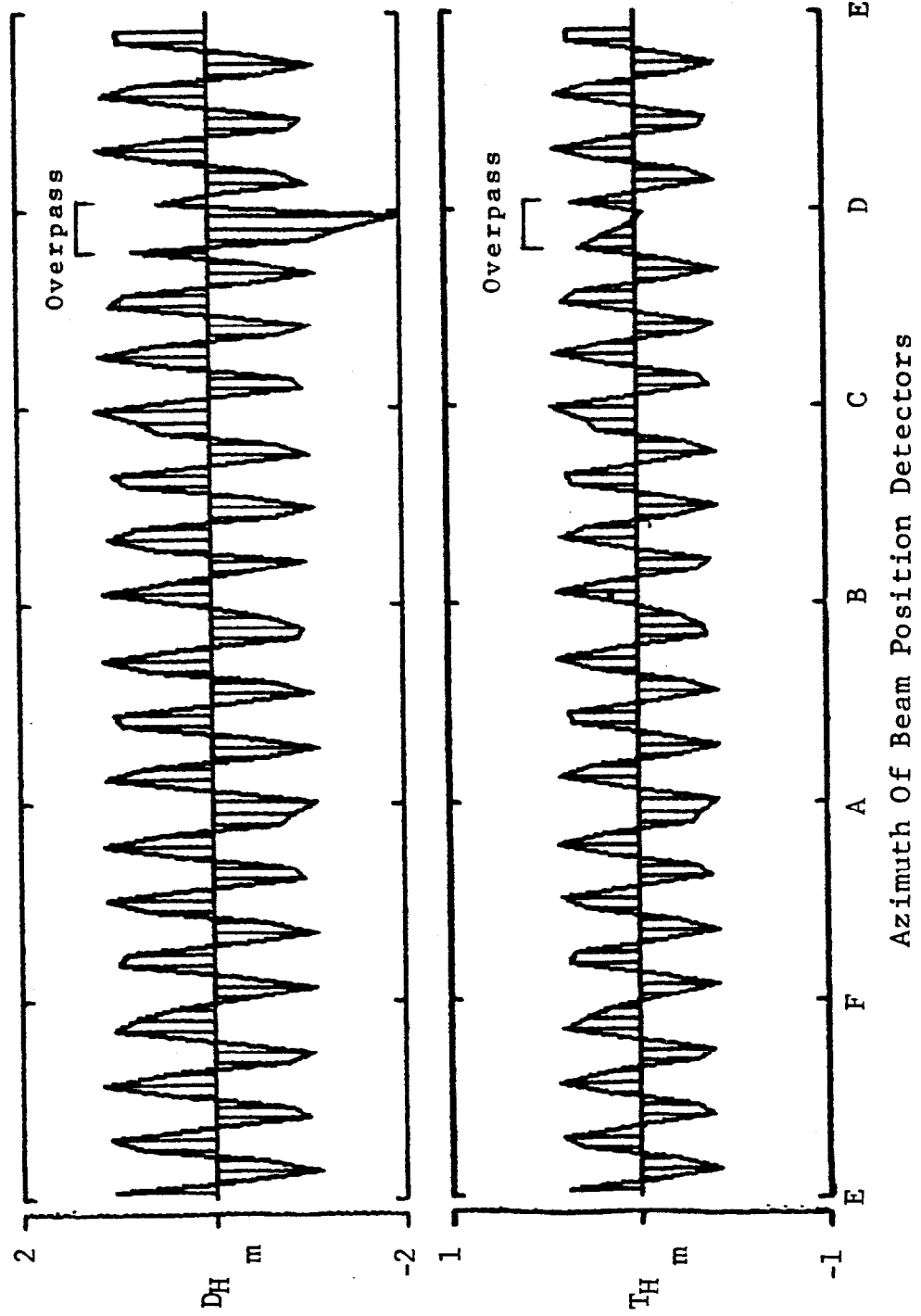
We summarize in Table I the numerical values of the various orbit distortion functions, including the horizontal and vertical momentum dispersion.

TABLE I

Distortion Function Summary

	<u>MAX</u>	<u>MIN</u>	<u><></u>	<u>RMS</u>
η_x	6.25	1.01	3.59	3.92 m
η_y	1.86	-1.77	~0	1.15 m
D_H	1.16	-1.16	~0	.824 m
T_H	0.44	-.44	~0	.303 m

Fig. 12

Main Ring Horizontal Distortion Functions with $D\theta$ Overpass

A global measure of the orbit distortion in Main Ring is given by the rms value of the orbit as recorded by the beam position detectors:

$$x_{\text{RMS}} = \sqrt{\frac{1}{108} \sum_i^{108} x_i^2}$$

$$y_{\text{RMS}} = \sqrt{\frac{1}{108} \sum_i^{108} y_i^2}$$
(19)

Typical values (before overpass) are 5 mm in x and 3 mm in y. To evaluate the sensitivity of x_{RMS} to δ_D , separate x_i into that due to the overpass, x_i^0 , and that due to errors elsewhere, \bar{x}_i ; so

$$x_i = \bar{x}_i + x_i^0 = \bar{x}_i + D_{Hi} \delta_D$$
(20)

Using Eq. (19) it is easy to show

$$x_{\text{RMS}} = \bar{x}_{\text{RMS}} \left[1 + 2\delta_D \frac{\sum \bar{x}_i D_{Hi}}{\sum \bar{x}_i^2} + \delta_D^2 \frac{D_{\text{HRMS}}^2}{\bar{x}_{\text{RMS}}^2} \right]$$
(21)

If the errors \bar{x}_i are not correlated with D_{Hi} , then for small δ_D

$$x_{\text{RMS}}(\delta_D) = \bar{x}_{\text{RMS}} \left[1 + \frac{1}{2} \frac{D_{\text{HRMS}}^2}{\bar{x}_{\text{RMS}}^2} \delta_D^2 \right]$$
(22)

Using the value from the Table I and $x_{\text{RMS}} = 5$ mm

$$x_{\text{RMS}}(\delta_D) = \bar{x}_{\text{RMS}} (1 + 0.0136 (1000 \delta_D)^2) \quad (23)$$

hence x_{RMS} is up 10% if $\delta_D = 0.0027$. Similarly for the vertical,

$$y_{\text{RMS}}(\delta_D) = \bar{y}_{\text{RMS}} (1 + 0.0735 (1000 \delta_D)^2), \quad (24)$$

so y_{RMS} is up 10% for $\delta_D = 0.00117$. For an increase by a factor $\sqrt{2}$ one has δ_D equal to .0061 and .0026 respectively. This indicates that one would like to control δ_D and δ_T with a precision of $\sim 0.1\%$.

In the above discussion it was assumed that similar dipoles on the same bus all have the identical bend angles; in practice "similar" dipoles may vary by $\pm 0.06\%$ at high field ($\pm 0.5\%$ at 8 GeV), giving rise to additional orbit distortions.

3. Tracking with Momentum

As described in Section III, the overpass design assumes that the eight bend magnets on the overpass bus have precisely twice the bend angle of a standard Main Ring dipole. The four purely horizontal bends are standard B1's and B2's; operation at $2 \times I_{\text{MR}}$ does not guarantee exactly twice the bend angle due to remnant field effects at 8 GeV and saturation effects at 150 GeV. The four vertical bends have substantially different geometry of coil and iron core, and are made from a different type of steel; hence, one might anticipate even larger deviations here. These are the reasons for the trim bus on the BV's and the two programmable currents in the power supply system, (see Sect. V), viz.

$$D\emptyset\text{DIFF} = D\emptyset\text{IB} - 2 I_{\text{MR}}$$

$$TD\emptyset\text{IB}$$

The "error" current, I_e , in the BV's will be the sum

$$I_e = D\emptyset\text{DIFF} + \frac{TD\emptyset\text{IB}}{1.2} = - 2 I_{\text{MR}} F(2 I_{\text{MR}}) \quad (25)$$

$$F(2I) = \frac{1/2 \int_{\text{BV}} B_y(2I) dl - \int_{\text{MR}} B_y(I) dl}{\int_{\text{MR}} B_y(I) dl} \quad (25a)$$

One can make a naive model for the momentum dependence of I_e at low field if we assume:

- (a) the field in the gap is the sum of remnant field, B^r , plus the field due to the current in the coil, $B = B^r + KI$.
- (b) the BV's have an effective strength, KL , that differs by δ from a MR dipole.

$$K_{\text{BV}} L_{\text{BV}} = K_{\text{MR}} L_{\text{MR}} (1 + \delta) \quad (26)$$

(c) no saturation effects,
then one can show

$$I_e(P) = \frac{2}{K} \left[B_{MR}^r - \frac{B_{BV}^r}{2} - 44.6 P \text{ (GeV/c)} \delta \right] \quad (27)$$

where B is in gauss and K is the constant relating current and field in the magnets,

$$B_{MR} = K I_{MR}, \quad K = 3.94 \text{ G/a} \quad (28)$$

Equation (27) gives a straight line as a function of P with slope related to δ and intercept to the difference in remnant fields.

In principle one could determine D \emptyset DIFF and TD \emptyset IB as a function of P by making precise magnetic measurements on all of the magnets, in practice it is more direct to use the beam closed orbit. One could imagine doing a grid search at each value of P for the values of D \emptyset DIFF and TD \emptyset IB that simultaneously give the minimum values for x_{RMS} and y_{RMS} ; it would be laborious. A better approach is to pick some reasonable starting values for D \emptyset DIFF and TD \emptyset IB, measure the resulting closed orbits, and then use our knowledge of the theoretical orbit distortion functions to predict the best values for D \emptyset DIFF and TD \emptyset IB.

Following Eq. (20) we can write the closed orbit position at the "i" location as

$$x_i = \bar{x}_i + \eta_{xi} \delta_p + D_{Hi} \delta_D + T_{Hi} \delta_T \quad (29a)$$

$$y_i = \bar{y}_i + \eta_{yi} \delta_p + D_{Vi} \delta_D + T_{Vi} \delta_T, \quad (29b)$$

where we have included all of the overpass distortion functions and the distortion $\eta\delta_p$ due to the momentum error of the beam ($\delta_p = \Delta P/P$). Using the relations of eq. (15), (29b) becomes

$$y_i = \bar{y}_i + \eta_{yi} (\delta_p - \delta_D - \delta_T) \quad (30)$$

The idea then is to do a least-squares-fit to $\{x_i\}$ with the function

$$\eta_{xi} \delta_p + D_{Hi} \delta_D + T_{Hi} \delta_T \quad (31)$$

i.e., we find the values of δ_p , δ_D , and δ_T that minimize

$$M_x \equiv \sum \bar{x}_i^2 \quad (32)$$

Similarly one can fit $\{y_i\}$ by

$$\eta_{yi} (\delta_p - \delta_D - \delta_T) \quad (33)$$

and find the value of $(\delta_p - \delta_D - \delta_T)$ that minimizes

$$M_y \equiv \sum_i \bar{y}_i^2 \quad (34)$$

The fit to $\{x_i\}$ determines all 3 parameters, whereas the fit to $\{y_i\}$ determines only the sum. Assuming there is no systematic roll angle error in the vertical dipoles (see VII 2. above), one could also choose to do a single combined fit, i.e. minimize

$$M = M_x + M_y \quad (35)$$

It is the last procedure (Ref. 10) that has been implemented and now exists as an on-line application program (Ref. 11) on M46, labeled "Main Ring Fit."

It should be mentioned that the solutions found for DØIB and TDØIB with the fitting program are not necessarily identical to the "zero distortion" values discussed in VII 2. above; it is only true if the closed orbit errors, \bar{x}_i , not associated with the overpass are not correlated to the errors arising from the overpass distortion.

VIII Magnetic Measurements of the Vertical Dipoles

The four vertical dipoles in the DØ overpass were designed specifically for the project. The important parameter is the large 3" gap between pole pieces in order not to restrict the horizontal aperture of Main Ring. Compared to a B1 type dipole it has twice the gap and four times the number of turns, hence, for the same current per turn it

gives twice the field and bending power of a B1. A list of design parameters (Ref. 4) is given in Appendix I.

The magnets were measured to full field (14 kG) utilizing the test stand and instrumentation normally used to measure Main Ring B1 and B2 magnets (Ref. 12). The basic probe is a 2-turn, long coil (1" wide by 260" long) that is connected to a precision voltage integrator. The test magnet is placed in series with the standard reference magnet (a 3' long B2-like magnet without vacuum chamber); the reference magnet has a 1" x 7" multiturn coil in the gap, whose output can be used to "buck" the output of the long coil in order to do relative measurements at the 0.001% level. The BV magnet design allows one to connect the top and bottom coils in series or in parallel by moving some jumper links on the manifold. The measurements reported here were made in the parallel mode; to the reference magnet, the BV then looks similar to a standard Main Ring bend, enabling a rather direct comparison.

In the measurements, the plane of the long coil was kept parallel to the pole surfaces and centered between poles. The measurements performed:

1. Linear current ramp from 0 to 4 ka, at 1900 a/s (7.5 kG/s or 84 GeV/s in Main Ring).
 - a) long coil bucked by reference coil, positioned at $x = 0"$, $\pm .5"$, $\pm 1.0"$, $\pm 1.5"$.
2. D.C. Measurements

- a) staircase current ramp 0 to 2.5 ka, bucked long coil at $x = 0''$.
- b) bucked long coil; .193, .50, 2.0 ka with $x = 0''$, $\pm .5''$, $\pm 1''$, $\pm 1.5''$.
- c) remnant field, rotate long coil; $x = 0''$, $\pm 0.5''$, $\pm 1.0''$, $\pm 1.5''$.

The results of $\int B dl$ measurements (1.(a) and 2.(a)) relative to the reference magnet are given in Fig. 13 (average of all four magnets), the error bars are the standard deviation. The curve out to 7.0 ka is an average of 120 MR bends (Ref. 13). The data indicate that the BV's are $\sim 0.6\%$ stronger than an average MR bend in the 1.0 to 2.5 ka range, visible saturation effects start at 2.5 ka, and at the 150 GeV/c level they are 0.3% stronger than average Main Ring. The difference between AC and DC measurements indicates an eddy current field of $\sim 6G$ at 7.5 kG/s. From Fig. 13 one can also conclude that the high field tracking between an average MR dipole at current I and $2I$ is quite good and that at the 150 GeV/c level the $2I$ is weaker by $\sim 0.08\%$.

From measurements 1.(a) and 2.(b) one can obtain the coefficients in a polynomial expansion of the midplane field, i.e.

$$B_y(x) = B_0 (1 + b_1 x + b_2 x^2 + b_3 x^3 + b_4 x^4) \quad (36)$$

The equations for obtaining the coefficients b_1 to b_4 from a finite width coil using the bucked data at $x = 0''$, $\pm 1''$, and $\pm 1.5''$ are given in Appendix II. In Fig. 14 we plot the coefficients for all four magnets. The points at 193 a (8 GeV level) are DC measurements, the rest are AC. At 8 GeV the quadrupole, b_1 , ranges between +3 and -1 (units of 10^{-4}

FIG. 13

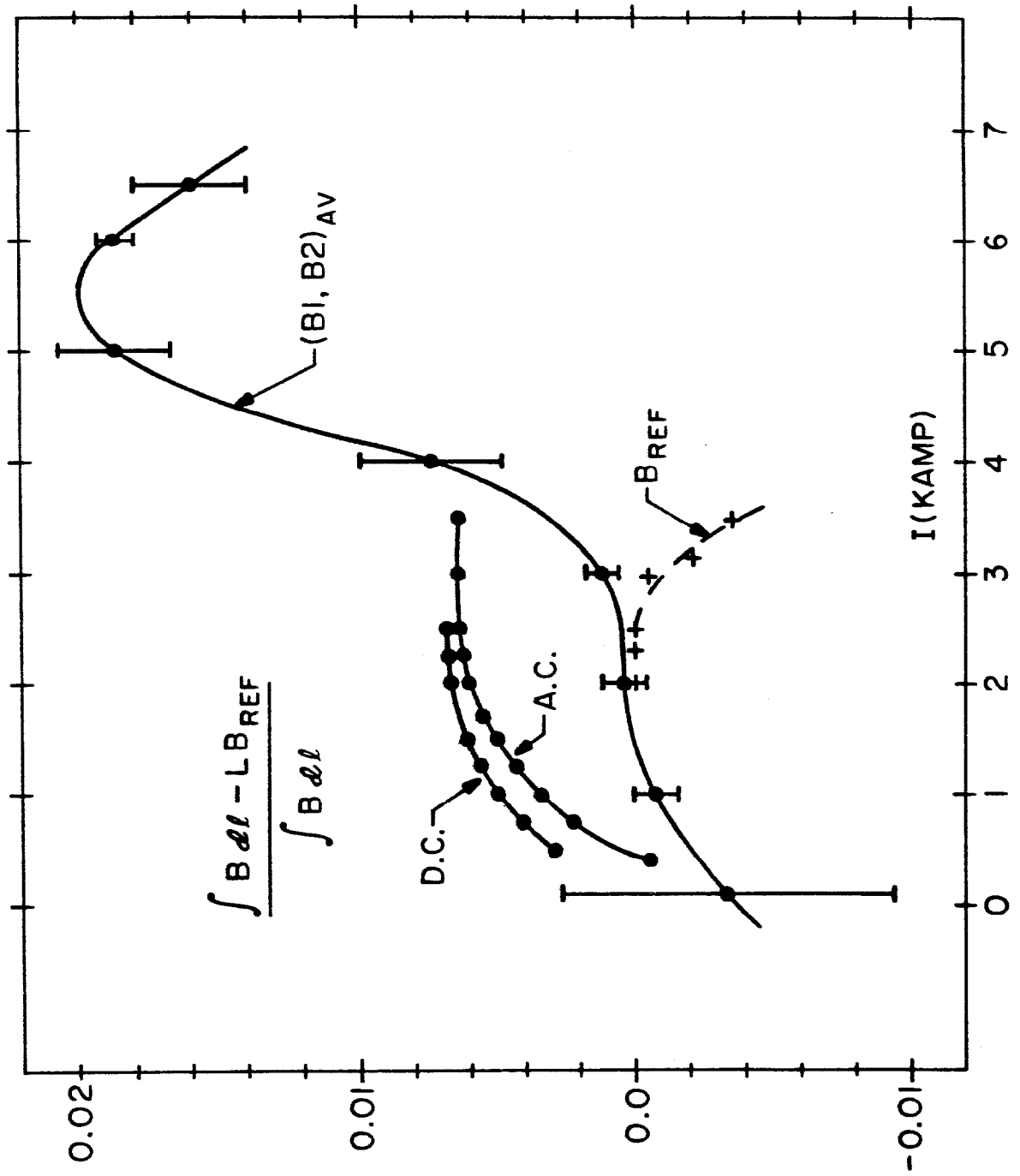
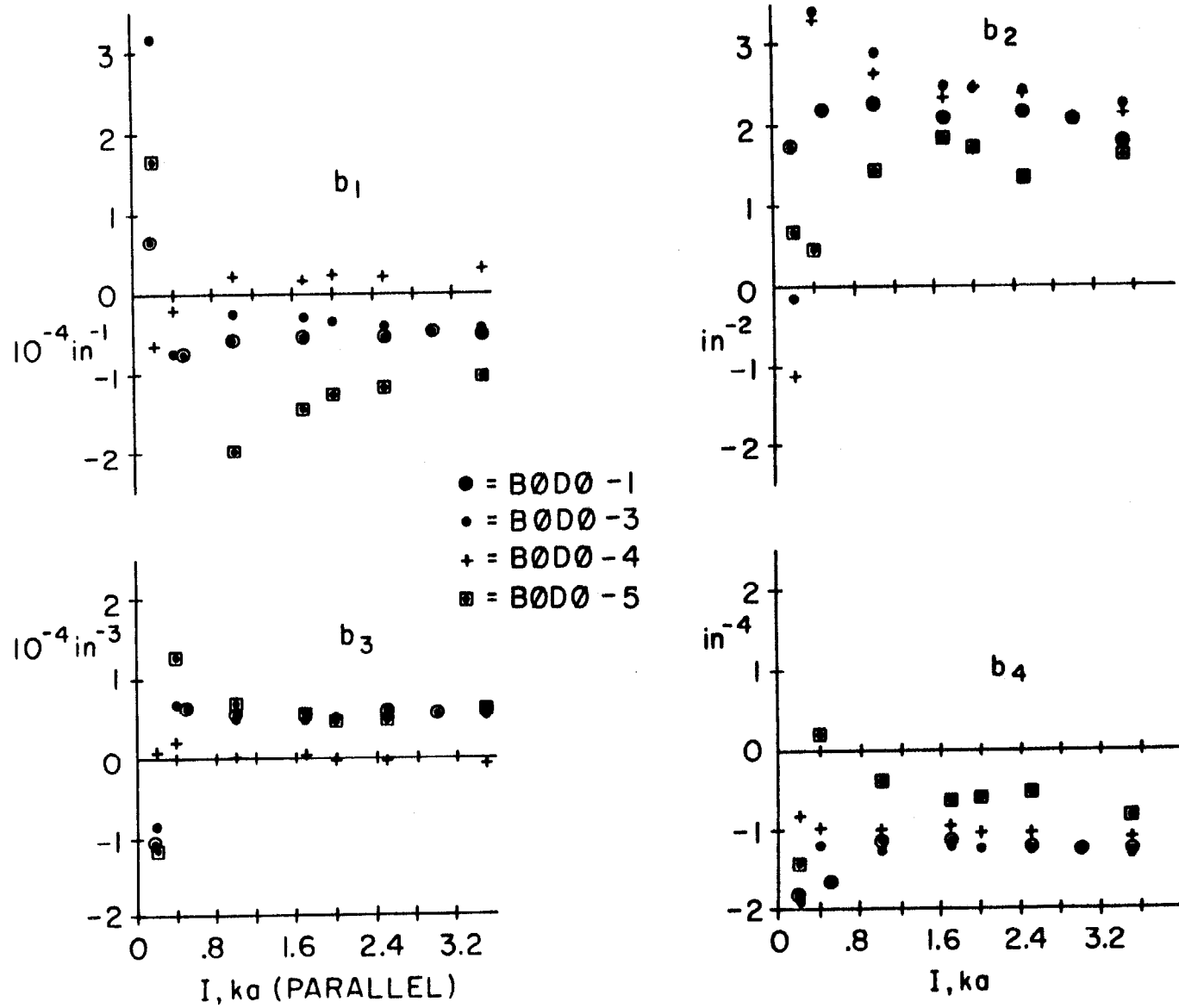


FIG. 14

Magnetic Field Coefficients Of Vertical Bend Magnets



in^{-1}) and the sextupole between +2 and -1. The data for BV serial #5 appear to have somewhat abnormal current dependence in b_1 , b_2 , and b_4 . In Fig. 15 we plot $B_y(x)$ using the average 3.5 ka values of b_2 and b_4 along with the predication of S. Snowdon (Ref. 4). B_y appears to be good to within 1 part in 10^4 out to $x = 1.5''$.

A summary of the remnant field measurements is given in Table II.

TABLE II

Magnet Serial Number	B (G)	b_2 (10^{-4} in^{-2})
1	24.5	-86
2	18.3	-88
3	21.5	-80
5	24.5	
	$\langle \rangle = 22.2 \pm 3$	-85

The remnant dipole field is large, (MR bends have 13 G in B2's and 17 G in B1's) about 2.8% of 8 GeV field, but not as large as the 3.8% for the average MR bend.

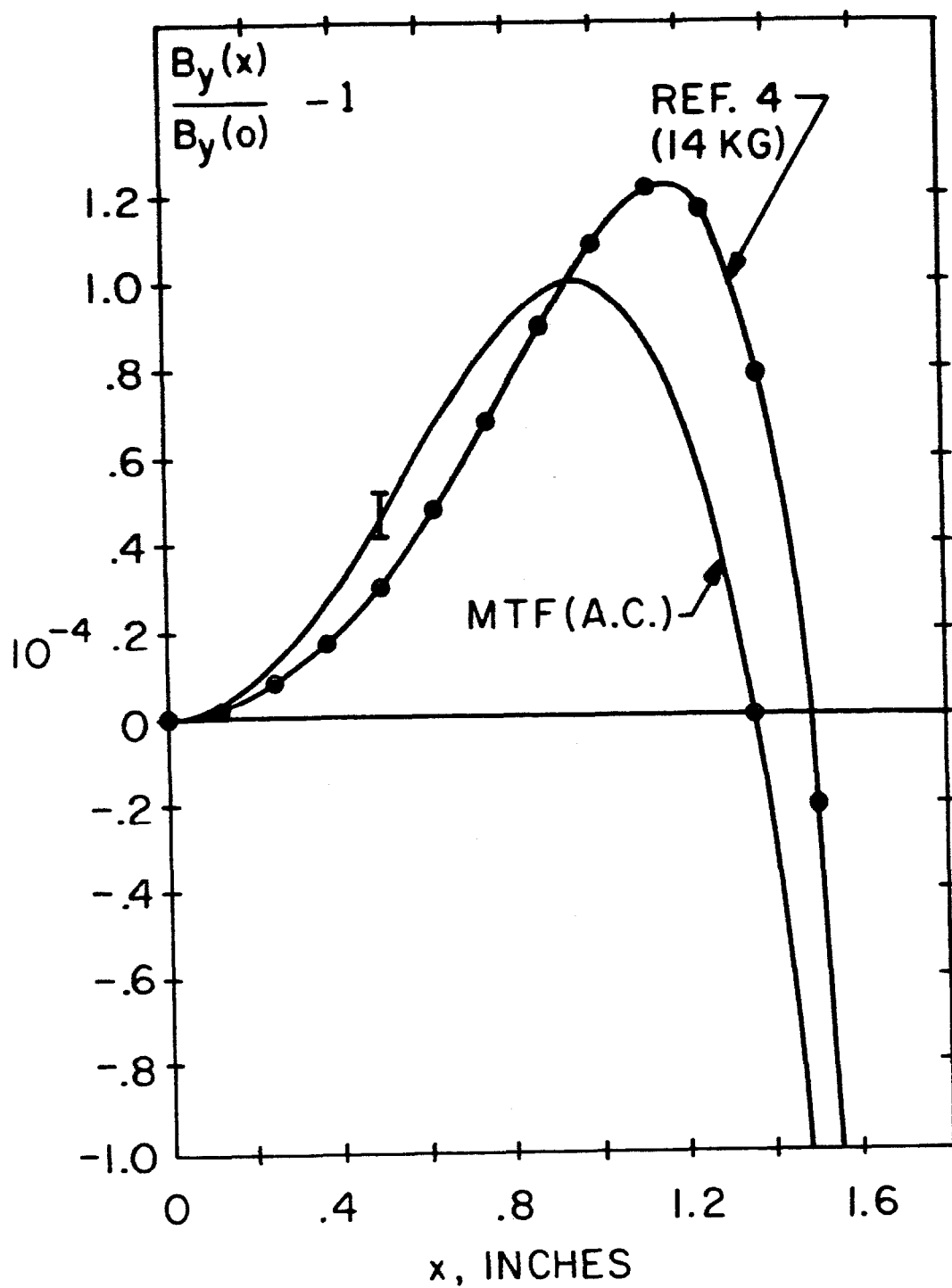
It should be noted that the measurements were not sensitive to possible skew field components in the magnets.

IX Initial Operating Experience with the Overpass

Circulating 8 GeV beam in the Main Ring with overpass was achieved for the first time on November 18, 1984. A few days later beam was accelerated to 150 GeV; this was done without using the trim windings on the vertical dipoles (TDØIB = 0a). The most striking (and expected) new

FIG. 15

Comparison Of Calculated And Measured Field
In Vertical Bend Magnet



feature was the dependence of the vertical closed orbit on $D\theta_{IB}$, a result of the nonzero vertical momentum dispersion created by the overpass; it was shown that η_y agreed with prediction (see Fig. 11(b)) to better than 10%. Following commissioning of the Trim Power Supply on November 25, a series of closed orbit measurements were performed in order to determine proper settings for both Main ($D\theta_{DIFF}$) and trim ($TD\theta_{IB}$) power supplies as a function of beam energy.

Variation of $D\theta_{IB}$, at fixed MR energy and $TD\theta_{IB}$, gave the expected parabolic behavior of x_{RMS} and y_{RMS} with δ_D as predicted by Eqs. (22) and (24). Early in December the "Main Ring Fit" program (see Sect. VII 3.) became available, which facilitated finding the optimum current-vs-energy programs for $D\theta_{DIFF}$ and $TD\theta_{IB}$. Fig. 16(a) shows the first set of curves derived in this way. The values at low energy (8-30 GeV) are clearly not unique, because there the MR correction dipoles can compensate for bend errors in the overpass magnets. In Fig. 16(b) we plot the error current, $I_e(P)$, as defined by Eq. (25) and draw in a straight line fit at low momentum.

On the basis of the magnetic measurements (Sect. VIII) and the discussion in Sect. VII, one can make the following observations concerning the data in Fig. 16.

1. In Fig. 17 we plot $I_e/2I_{MR}$ versus $2I_{MR}$; the curve is the field integral difference between the average BV at $2I_{MR}$ and an average BH at I_{MR} (the quantity $F(2I_{MR})$ defined in Eq. (25(a)) as derived from the MTF magnetic measurements (Ref. 12 and Fig. 13). The agreement between the two sets of data is quite

FIG. 16

Overpass Main And Trim Currents For Momentum Tracking

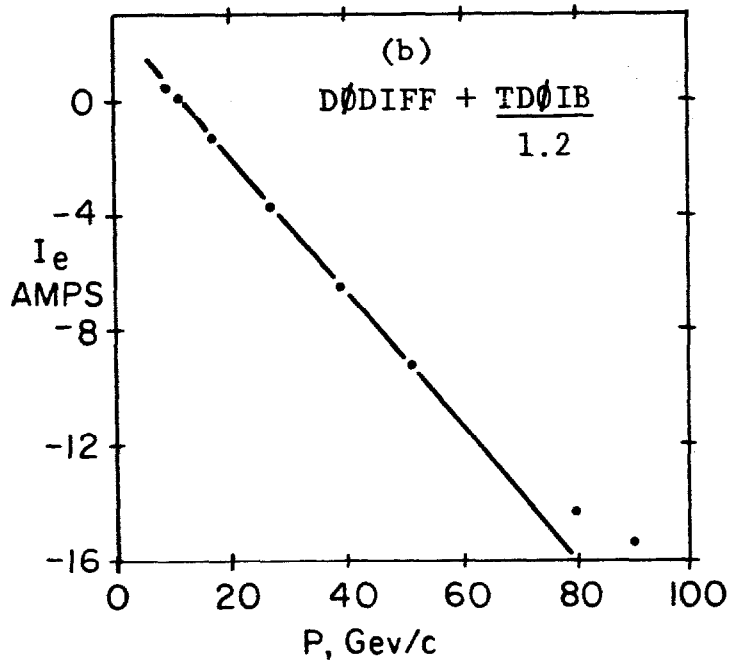
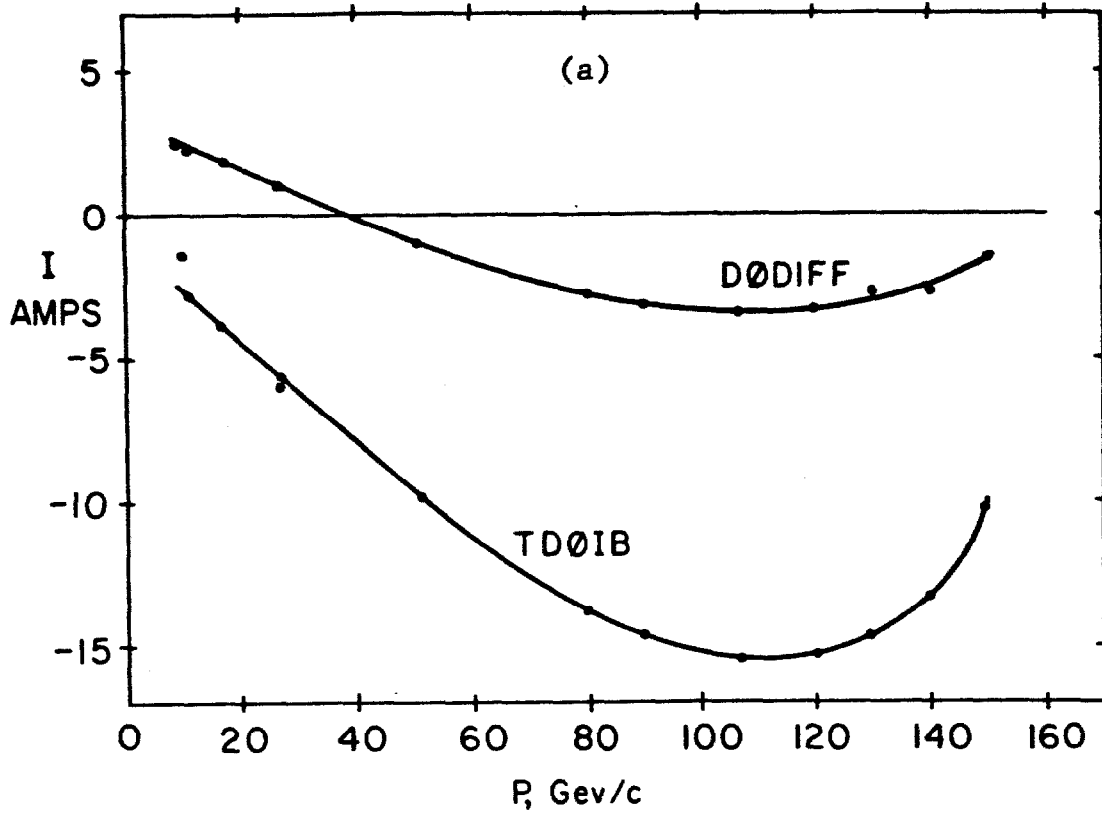
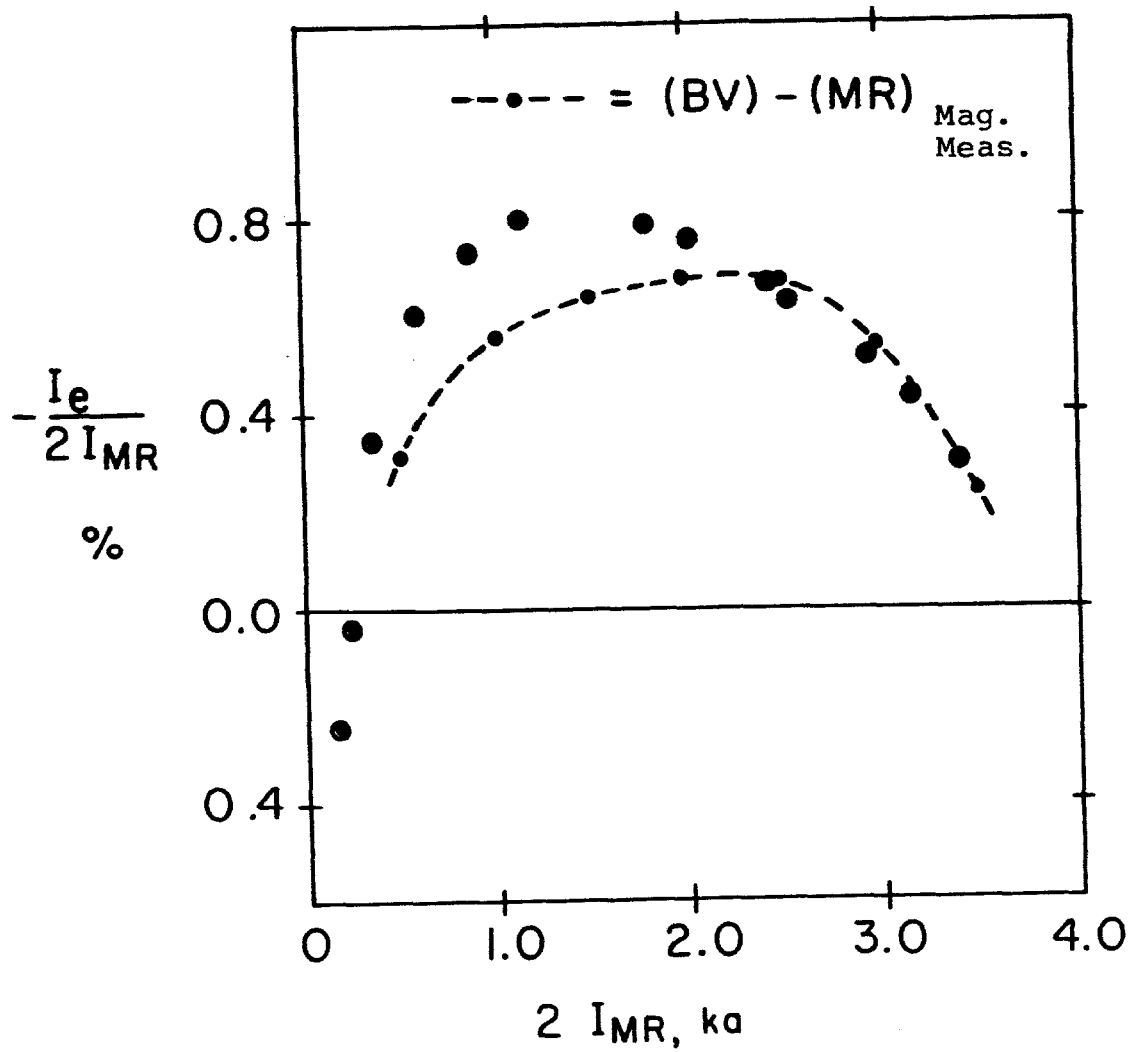


FIG. 17

Comparison Of Vertical Bend Momentum
Tracking With Magnetic Measurements



reasonable. The vertical bends are 0.8% too strong, predominantly an effective length effect; the sign reversal at low field is a remnant field effect (see below) and saturation effects become evident above 90 GeV/c (2 ka).

2. It is possible to understand the sign and approximate value of $D\theta_{DIFF}$ at 8 GeV in terms of remnant fields. Since the remnant field of a MR dipole is nearly independent of peak current (Ref. 14), $\langle B_{MR}^r \rangle = 15$ G, the BH2X bends on the overpass will have a deficit of ~ 15 G at 8 GeV for $I = 2I_{MR}$. Since $k \approx 4G/a$, we expect $D\theta_{DIFF} = + 3.7$ a at 8 GeV, assuming the deficit is not supplied by the MR correction dipoles. We can get the sign and magnitude of I_e using Eq. (27); from the slope of the line in Fig. 16(b) we find $\delta = + 1.0\%$. Using the measured $\langle B_{BV}^r \rangle$ of the BV's of 22G, Eq. (27) gives $I_e \approx 0$, hence one expects

$$TD\theta_{IB} = 1.2 D\theta_{DIFF} \approx -4.4a. \quad (37)$$

During the first few weeks of operation of the Main Ring with the overpass, beam measurements at 8 GeV indicated a fairly strong coupling between horizontal and vertical betatron motion originating in the region of the overpass. Subsequent studies (Ref. 15) revealed the coupling to be an artifact of misaligned correction sextupoles.

Experience so far shows that the closed orbit quality achievable in the Main Ring has not been appreciably affected by the presence of the overpass.

X Overpass Beam Dynamics Effects

1. **Horizontal-Vertical Coupling Effects** - An overpass with "screw" geometry that contains quadrupoles will introduce coupling between the horizontal and vertical betatron motions (Ref.16). The betatron motion, which is in the vertical plane in the ring outside of the overpass region; deviates from the vertical plane by a small angle in traversing the overpass region, since the quadrupoles in the overpass have zero roll angle, this will generate a linear coupling between the horizontal and vertical motions. That is, if one kicks the beam horizontally at a point in the ring outside of the overpass region then a response in the vertical will be observed. The angle of rotation of the "vertical" motion (rotation around the beam direction) in the overpass region is a function of the horizontal position in the overpass and is given by (Ref.16)

$$\theta_{Ri} = \sum_j \theta_{v_j} \phi_j \quad (38)$$

where ϕ_j is the bend angle of the nonrolled dipoles, and the sum extends over the overpass dipoles upstream of the point of interest; θ_{v_j} is the pitch angle of +15.76 mrad going up the slope and -15.76 coming down. Hence θ_R increases from zero at C46 to a maximum of ~1.1 mrad at D0 ("vertical" tilts inwards toward center of ring) and then decreases back to zero at D14. (It is of interest to note that there is one less zero roll dipole coming up

the slope than going down due to the missing dipole at C48-2.) In effect, it is as if the quads at C49 and D11 were rolled 1.1 mrad (wall side down) and the ones at C48 and D12 about 0.6 mrad. (A 1 mrad roll of a standard 7' quad gives a 0.76 μ rad vertical kick per cm of horizontal displacement, a fairly small effect.) Obviously any normal component quadrupole fields in the nonrolled dipoles would also contribute to linear coupling.

Another potential source of coupling is the existence of higher order fields in the new rolled vertical bends. Clearly normal quad or skew quad would contribute (Ref.15). The presence of a normal sextupole (normal in the sense of the main field in the dipole) will give an effective skew quadrupole which goes linearly with the horizontal displacement of the closed orbit in the BV dipoles.

2. Other Effects

Although the local experts suggest that the impact of the overpass on beam dynamics should be "small", it has not yet been very carefully studied. One effect that has been mentioned by S. Ohnuma is the momentum-dependent coupling between horizontal and vertical as a result of finite vertical dispersion and the presence of normal sextupole around the ring.

XI Overpass Impact on Main Ring and Tevatron Capabilities

Potential harmful effects of the overpass on Main Ring and Tevatron performance have been considered by S. Ohnuma (Ref.8,17).

1. Injection efficiency into Main Ring (8 GeV acceptance) -

a) Assuming that closed orbit distortions due to overpass dipole variations can be eliminated with the MR correction dipole system, no loss of aperture should occur from this effect.

b) Loss of efficiency due to increased size of circulating beam (for a given transverse emittance from the Booster).

1. Increased H and V beam size due to H-V coupling effects intrinsic to the screw overpass geometry. In Ref.8 this is estimated to be a 5% effect for the proposed B0 overpass (it has ~4 times the coupling of the smaller D0 overpass).

2. Increased V beam size due to vertical momentum dispersion. For an ϵ (95%) = 2π mm-mrad and a $\Delta p/p = +0.1\%$, the beam size at $\beta_y = 100$ m and $\eta_y = 1.7$ m (occurs at many B2 dipoles) will increase by 4%. A similar increase takes place at the C0 and E0 Lambertson magnets where $\beta_y \sim 124$ m.

3. Increased vertical beam size due to a vertical momentum dispersion mismatch between the 8 GeV line from Booster and Main Ring at A0, a dilution of the vertical emittance results. The mismatch due to the D0 overpass is ~1 m, which should give less than a 1% increase in size.

2. Acceleration efficiency in Main Ring - It is not unusual to have shifts in radial position early in the acceleration cycle corresponding to momentum errors $\sim 0.1\%$, in addition there is a transient increase in momentum spread at transition ($\Delta p/p \sim \pm 0.2\%$, depends on RF voltage). With $\eta_y \neq 0$, these effects will cause closed orbit distortions and an increase in vertical beam size. The combination of vertical effects and radial shifts may well degrade the acceleration efficiency at high intensity.
3. Luminosity for $\bar{p}p$ collisions in the Tevatron - Any vertical dispersion mismatch between Main Ring and Tevatron at E_0 , where the 150 GeV transfer of both p and \bar{p} takes place, will also dilute the vertical emittance giving a larger vertical beam at the collision point, hence lower luminosity. The discussion in Ref.17 indicates a 1.8 m mismatch due to the D_0 overpass with a consequent 12% reduction in luminosity.

XII Summary

The recent successful operation of the Main Ring with the D_0 overpass has confirmed the statement of Tom Collins (Ref.1) made nearly four years ago, viz. "a technically sound by-pass can be built, which is simple to operate". At the time of this writing, the Main Ring - Tevatron complex has been running the 800 GeV fixed-target experimental program for eight weeks. Beam intensity as high as 1×10^{13} ppp has been delivered to the experimental targets, equivalent to the best pre-overpass performance. Within the limited operational experience to

date, the overpass system - including magnets, power supplies, controls, and tuning capability - has proven to be reliable and effective.

The DØ overpass as implemented deviates from the proposal of T. Collins in two respects: (a) special vertical bend dipoles with 2.8 inch aperture were built as opposed to using MR B2 magnets with 1.9 inch aperture and (b) for pragmatic reasons the geometry which gives zero vertical momentum dispersion outside of the overpass region was not used, resulting in an η_y with RMS value of 1.15 m. The first deviation was clearly the proper choice; although existing evidence supports the wisdom of the second choice, its full impact on high intensity operation and $\bar{p}p$ operation remains to be evaluated.

The actual commissioning of the overpass occurred over a four week period of general accelerator startup, and everything considered, went rather smoothly. The modifications to the lattice functions of the Main Ring due to the overpass appear to be close to prediction. The very large horizontal-vertical coupling observed during the initial operation with the overpass was not due to the overpass per se; the possibility of some residual coupling coming from higher order fields in the new vertical bend magnets remains to be explored. Present operational experience suggests that the closed orbit quality and transmission efficiency through Main Ring has not been appreciably altered by the presence of the overpass.

Acknowledgements

The DØ overpass project was a substantial effort, much of the work described here was done by others. I am grateful to Craig Moore, Stan Pruss, Don Edwards, Mel Month, Rod Gerig, Howard Pfeffer, Bill Merz, Mike May, Stan Snowdon, Dean Krause, Jim Crisp, and Jim Garvey for providing me with information derived from their work. Above all I should acknowledge Sho Ohnuma, the conceptual parent of the DØ overpass, for many discussions which were usually entertaining, if not always enlightening.

Finally, I am indebted to Carolyn Merkler for her good work and patience in the typing of this report.

References

1. T. Collins, "A By-Pass for the Main Ring around B \emptyset (or D \emptyset) after Doubler Operation," June 1981.
2. S. Ohnuma, "Collin's Bypass for the Main Ring," TM-1124, August 10, 1983.
3. Private communication with C. Moore, November 1984.
4. S.C. Snowdon, "Overpass Vertical and Horizontal Dipoles," memo to F. Turkot, October 8, 1984.
5. Private communication with H. Pfeffer and W. Merz, November 1984.
6. C. Ankenbrandt and H. Pfeffer, "Matching Fermilab Main Ring and Tevatron Guide Fields," Proceedings of the 12th International Conference on High-Energy Accelerators, 1983.
7. Private communication with R. Gerig, November 1984.
8. S. Ohnuma, "Calculation of Lattice Parameters for the Main Ring with B \emptyset Overpass," \bar{p} Note #318, July 1983. The computer program B \emptyset SYNCH described in this report has been used to calculate lattice parameters for the WD51D2 geometry of the D \emptyset overpass, private communication with S. Ohnuma, November 1984.
9. M. Sands, "The Physics of Electron Storage Rings, An Introduction," Course XLVI, Proceedings of the International School of Physics, Academic Press (1971).
10. These functions were first calculated by D. Edwards, in memo "Minimization of Orbit Distortion Using Overpass Supplies," November 25, 1984.

11. Private communication with R. Gerig, December 1984.
12. D. Krause, "Magnet Measurement for Overpass Section at DØ," memo to S. Ohnuma, C. Moore, F. Turkot, December 1984.
13. J. Crisp, "The Momentum of Main Ring Beam as a Function of Magnet Current," TM-814, October 1978, the curve of Fig. 13 was provided by J. Crisp.
14. R. Juhala, "Variation of Remnant Field with Peak Excitation in MR B2 Magnets," TM-488, May 15, 1974.
15. F. Turkot, "Studies of Horizontal-Vertical Betatron Coupling in the Main Ring Following the November 1984 Startup," EXP-116, February 11, 1985.
16. M. Month, "Beam Model for Non-Planar Orbits in Synchrotrons," AGS Division Report 84-2, DØ Note #64, March 26, 1984.
17. S. Ohnuma, "Main Ring Overpass: Issues (But Not Answers) As I See Them," memo of August 18, 1983.

APPENDIX IOverpass Vertical Bend Dipole Design Parameters

Field Strength	14 kG
Magnet Length (iron)	236.88 in.
Magnet Gap.....	3.00 in.
Physical Aperture	5.00 in.
Field Aperture	3.00 in.
Field Quality.....	+0.01 percent
Coil Turns (w/o trim)	24/pole
Copper Conductor Cross Section	0.793 in. by 0.654 in.
Water Cooling Hole <u>Diameter</u>	0.325 in.
Conductor Corner Radius	0.094 in.
Ampfac	1.0024
Conductor Current (series).....	1773A
Magnet Length (effective)	240 in.
Magnet Inductance (series)	0.0601 H
Coil Resistance (series).....	0.0456 Ω
Voltage Drop	80.9 V
Power (33 percent duty factor)	47.8 kW
Cooling Water Pressure.....	65 psi
Number of Water Paths	6
Water Flow	13 GPM
Temperature Rise.....	14 ^o C
Outside Dimensions	29 in. by 17 1/2 in.
Iron Weight	26100 lbs
Copper Weight.....	3488 lbs
Trim Coil Turns	10/pole
Trim Conductor, Copper	0.225 in. x 0.225 in.
Vacuum Chamber Material.....	0.090 in. of 316 stainless
Beam Aperture	2.8 in. by 4.7 in.

APPENDIX II

Midplane Field Coefficients for Finite Width Coil

We want to find the coefficients b_i in the midplane expansion of B_y ,

$$B_y(x) = B_0 (1 + b_1 x + b_2 x^2 + b_3 x^3 + b_4 x^4) \quad (1)$$

given measurements with a coil of width W and center at \bar{x} ; the basic data used consisted of measurements at $\bar{x} = 0''$, $\pm 1.0''$, $\pm 1.5''$. Since $W \neq 0$ we obtain "average" fields {call them $\bar{B}(\bar{x}_i)$ } at these values of \bar{x} ; the raw data provided by the measurement procedure is then:

$$\left\{ \frac{\bar{B}(\bar{x}_i) - \bar{B}(0)}{\bar{B}(0)} \right\} \quad (2)$$

From these 5 numbers we form the following differences and sums:

$$d \equiv \frac{\bar{B}(1) - \bar{B}(-1)}{\bar{B}(0)} ; \quad D \equiv \frac{\bar{B}(1.5) - \bar{B}(-1.5)}{\bar{B}(0)} \quad (3)$$

$$s \equiv \frac{\bar{B}(1) + \bar{B}(-1) - 2\bar{B}(0)}{\bar{B}(0)} ; \quad S \equiv \frac{\bar{B}(1.5) + \bar{B}(-1.5) - 2\bar{B}(0)}{\bar{B}(0)}$$

To find the response, $W \bar{B}_m(\bar{x})$, of the coil to the x^n term of Eq.

(1) we have

$$W \bar{B}_n(\bar{x}_o) = b_n \int_{\bar{x}_o - \frac{W}{2}}^{\bar{x}_o + \frac{W}{2}} x^n dx = \frac{b_n}{n+1} \left[(\bar{x}_o + w/2)^{n+1} - (\bar{x}_o - w/2)^{n+1} \right] \quad (4)$$

Hence the full response at $\bar{x} = 1''$, $1.5''$ and $W = 1''$ becomes:

$$\frac{\bar{B}(1) - \bar{B}(o)}{B_o} = b_1 + 1.08 b_2 + 1.25 b_3 + 1.51 b_4 \quad (5)$$

$$\frac{\bar{B}(1.5) - \bar{B}(o)}{B_o} = 1.5b_1 + 2.33 b_2 + 3.75 b_3 + 6.20 b_4$$

(where we have ignored $W \neq 0$ at $\bar{x} = 0$); the equations for $x = -1$ and -1.5 are obvious.

Using Eqs.(3) and Eqs.(5) one can then solve for b_i in terms of d, D, s , and S giving:

$$\begin{aligned} b_1 &= 1.0 d - .33D ; & b_3 &= - 0.40d + .27D \\ b_2 &= 0.97s - .24S ; & b_4 &= - 0.37s + 0.17S \end{aligned} \quad (6)$$